Crystalline, Shape, and Surface Anisotropy in Two Crystal Morphologies of Superparamagnetic Cobalt Nanoparticles by Ferromagnetic Resonance

Michael R. Diehl, Jae-Young Yu, and James R. Heath*

UCLA Department of Chemistry and Biochemistry, 405 Hilgard Ave., Los Angeles, California 90095-1569

Glenn A. Held, Hugh Doyle, Shouheng Sun, and Christopher B. Murray

IBM T. J. Watson Research Center, P.O. Box 218, Yorktown Heights, New York 10598

Received: November 20, 2000; In Final Form: April 17, 2001

Ferromagnetic resonance (FMR) techniques are used to investigate superparamagnetic cobalt nanoparticles (NP's) with different crystalline structures and sizes ranging from 4 to 9 nm in diameter. Magnetic contributions from NC shape, crystallographic structure, defects, and surface structure are discussed. An independent-superparamagnetic-grain model is employed to simulate the FMR measurements. The results from both single crystalline and polycrystalline cobalt NP's reveal that a particle's effective anisotropy, and thus its magnetic properties, are extremely sensitive to internal structure as well as overall particle shape. Finally, surface chemical properties were found to yield unique FMR signatures for NP's at low temperatures.

I. Introduction

In magnetic materials, below some critical size, individual nanoparticles (NP's) within a dispersion can each support only a single magnetic domain, and so can each be viewed as a single large magnetic moment. At low temperatures (T), this moment is pinned along one of the "easy," energetically favorable axes of the particle, whereupon a particle dispersion exhibits ferromagnetic behavior. Above some blocking temperature, however, thermal fluctuations can overcome the anisotropy barrier, so the moments can rotate among the different easy directions. The dispersion is then said to be superparamagnetic.[1] As the total moment of each NP scales directly with its volume, the scaling properties observed for these systems are fundamentally different from those observed in bulk magnetic systems.

The magnetic anisotropy observed in NP's has a number of components. These include magnetocrystalline, shape, and surface anisotropies. According to the model of Néel[2] and Brown[3], the remnant magnetization of an ensemble of non-interacting, single domain NP's should decay as$\langle scp\rangle$ $M(t) \propto e^{-t/\tau}\langle mx\rangle$, as a function of the time t following the removal of a saturating magnetic field. In this expression $\langle scp\rangle$ $\tau \equiv f_0^{-1}$ e^{KV/k_BT},$\langle mx\rangle$ K is the anisotropy energy barrier density, V is the NP volume, and the attempt frequency$\langle scp\rangle$ $f_0\langle mx\rangle$ is assumed to be 10^9-10^{12} Hz. It follows from the double exponential dependence of $M(t)$ on the product KV, that even a modest distribution of anisotropy or volume among the particles in a dispersion will result in a significant broadening of the ferro- to superparamagnetic transition. Thus, an essential requirement for any experiment attempting to characterize the magnitude and components of the NP anisotropy is the ability to prepare a highly uniform dispersion of magnetic NP's. Due to the diverse sources of anisotropy, a complete realization of size-dependent scaling laws in magnetic systems requires an understanding of the influence of the unit cell symmetry of the crystal lattice, the coherence of the crystal lattice throughout the particle, and the shape and surface composition of the particle.

Chemical syntheses have been recently reported for the growth of NP's comprised of Co cores that are surfactant stabilized by oleic acid.[10] Size selective precipitation of these NP's leads to highly uniform particle size distributions with median diameter ranges between 4 and 9 nm and a spread in particle diameters of from 5 to 10%. Depending upon the synthetic route followed, the NP's can be formed as either an ϵ-Co cubic phase or with a multiply twinned fcc-based icosahedral (mt-fcc) crystal symmetry (Figure 1). The ϵ-Co structure, which is not observed in the bulk, consists of a twenty-atom unit cell with cubic symmetry similar to the structure of β-Mn.[4] TEM measurements indicate that these particles possess distinct crystal facets on the surface, and atomistic simulations[5] of TEM and X-ray powder data indicate that the ϵ-Co NP's are nearly perfect single crystals (Figure 2). By contrast, the mt-fcc NP's are characterized by sharp boundaries of image contrast when probed by TEM, indicating that these particles are broken into domains. Atomistic X-ray modeling shows that the particles are multiply twinned, where each particle is comprised of crystallographic plane-sharing polyhedra, and the crystallite subdomains consist of a distorted fcc lattice. X-ray data indicates the polyhedra are not perfect, but rather they contain various stacking and twinning faults. This structure is similar (albeit more highly defective) to what is observed in multiply twinned, icosohedral gold particles.[6]

Both NP crystal morphs appear to be characterized by a mixed cobalt oxide surface layer to a depth of approximately 2 lattice planes. We will consider the neutral metallic volume, as determined by X-ray, to be the actual magnetic volume of the particle, although we will return to the surface oxide and its signatures at the end of this paper.

For NP's with either of these crystalline structures, analysis of remnant magnetization from SQUID magnetometry data yields an effective anisotropy with uniaxial symmetry.[7] That

* Author to whom correspondence should be addressed. E-mail: heath@chem.ucla.edu.

10.1021/jp004252y CCC: $20.00
Published on Web 07/20/2001

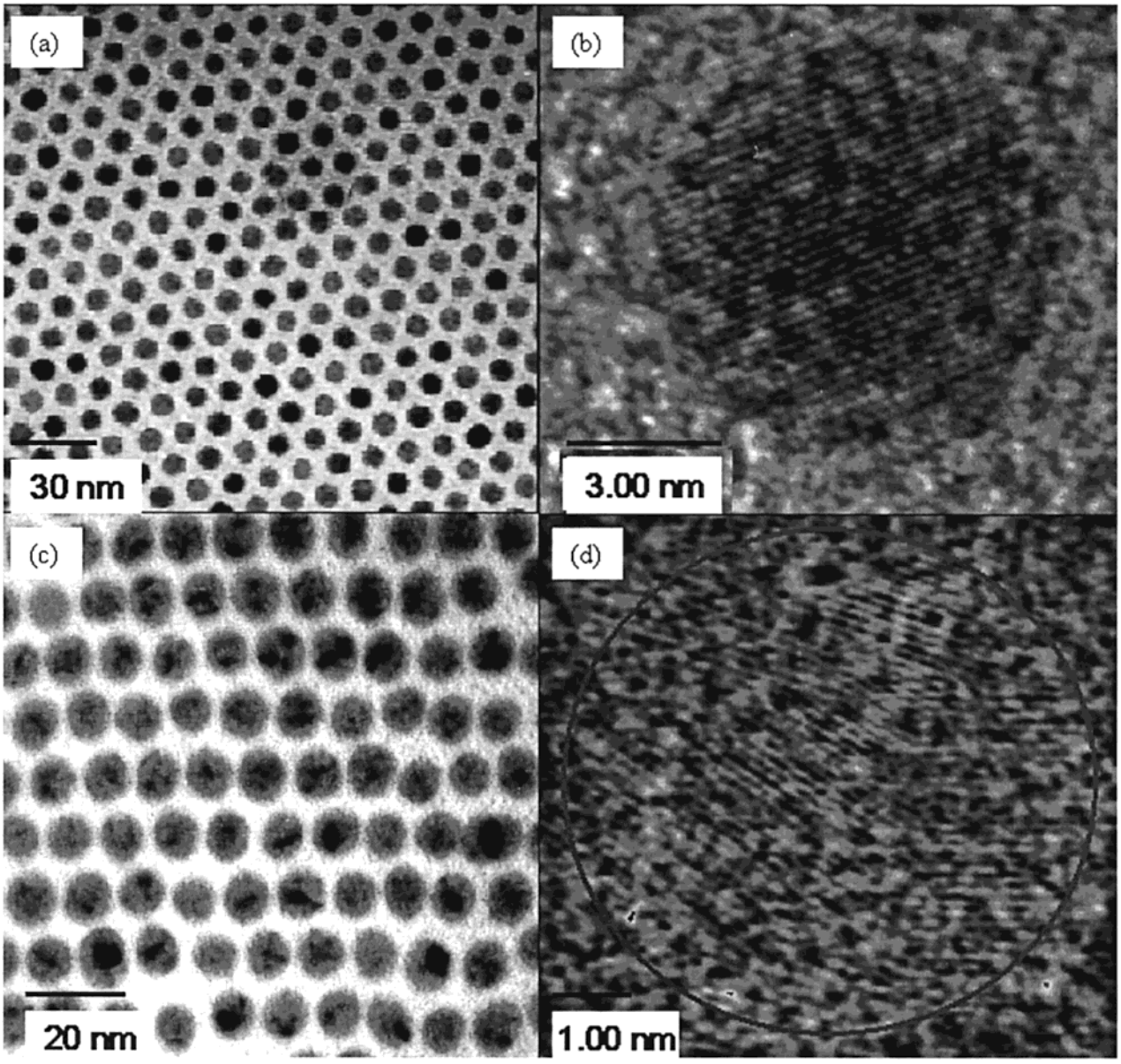

Figure 1. TEM images of the phases of cobalt nanoparticles examined here. (a) Low magnification image of ϵ-Co. The even contrast across the individual particles implies a uniform crystalline structure for this phase. (b) HRTEM image of ϵ-Co showing perfect crystallographic coherence and discrete faceting, which leads to a shape anisotropy. (c) Low magnification image of mt-fcc structure. Contrast changes within particles indicate they are comprised of crystal domains. (d) HRTEM showing the domains within a single mt-fcc particle. These domains correspond to a multiply twinned structure.

is, SQUID measurements neither reflect the crystallographic symmetry of the particles, nor do they reveal any qualitative differences in the magnetic properties of ϵ-Co and mt-fcc structured NP's. This result is interpreted as an indication that shape anisotropy makes the predominant contribution to the overall anisotropy of NP's with either crystal symmetry.

In this paper, we present an FMR study of these highly uniform, chemically synthesized magnetic NP's. We collected FMR data from NP's as a function of particle structure, size, and temperature. We compare the results obtained from ϵ-Co and mt-fcc NP's in an effort to develop a comprehensive picture of the effects of crystalline structure and particle shape on the overall NP anisotropy. We interpret our spectra within the framework of Raikher and Stepanov's independent-superparamagnetic-grain model.[8,9] Finally, we present low-temperature data which suggests the presence of surface anisotropy contributions to the magnetic response of ϵ-Co NP's.

II. FMR in Superparamagnetic Particles

FMR of magnetic NPs differs from resonance behavior in bulk materials since the skin depth greatly exceeds the particle size, and multi-magnetic domain structure is excluded from line shape. Here, FMR is characterized by a uniform precession about the Larmor frequency (ω_r) given by eq 1:

$$\omega_r = \gamma H_{eff} \tag{1}$$

where γ is the gyromagnetic ratio and H_{eff} is the effective field. H_{eff} is comprised of the anisotropy field (H_a), fluctuation field (H_f), and the applied field (H_{ap}). The anisotropy field depends on the orientation of the particle easy axis with respect to the applied field. The fluctuation field accounts for thermal dephasing associated with the superparamagnetic state.

Raikher et al. have previously reported an analytical calculation of the fluctuation and anisotropy field in NP's. They utilized

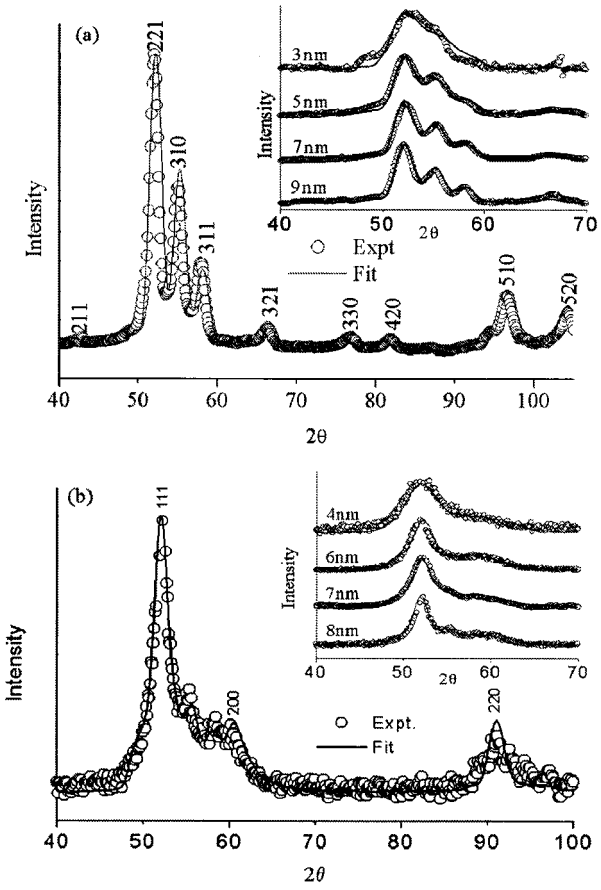

Figure 2. X-ray data (circles) for cobalt nanoparticles and their corresponding simulations (solids lines) using atomic-level models of the particles. (a) ϵ-Co, (b) mt-fcc particles. The insets are X-ray data and simulations for several particle sizes.

a truncated series of spherical harmonics to approximate the anisotropy field and then used the resulting expressions to solve the Landau-Lifshitz equation (LLE) for the dynamical susceptibility. Considering conventional FMR techniques, where the spectrometer frequency is static and the applied field is swept, this procedure yields expressions for the resonance field for a given orientation of a particle with respect to the applied field:

$$H_{\text{uniaxial}} = \frac{\omega}{\gamma} - 2\frac{K_2}{M_s}\frac{L_2(\xi)}{L_1(\xi)}P_2(\cos(\theta)) \tag{2}$$

$$H_{\text{cubic}} = \frac{\omega}{\gamma} - 2\frac{K_4}{M_s}\frac{L_4(\xi)}{L_1(\xi)}\left(1 - \frac{5}{4}\sin^2(2\theta) - \frac{5}{4}\sin^4(\theta)\sin^2(2\phi)\right) \tag{3}$$

where ω is the spectrometer frequency, K_2 and K_4 are uniaxial and cubic anisotropy constants, respectively, and P_j are the Legendre polynomials of order j. The functions L_j in eqs 2 and 3 correspond to the family of Langevin functions with the argument $\xi = \mu H/k_b T$, where μ is the particle moment, and H is the applied field. The full line shape function is averaged over all individual susceptibilities (χ) weighted by an orientational distribution function:

$$\bar{\chi}(\omega, H_{\text{ap}}) = \int \chi(\theta,\phi) f(n_\theta, n_\phi) \tag{4}$$

where $f(n_\theta, n_\phi)$ is the "orientation texture" of the particle's anisotropy axes.[9]

For an isotropic distribution of particle axes, changes in line shape and line-broadening with respect to temperature or particle size reflect the competition of the anisotropy field H_a and the fluctuation field H_f. For large particles and/or low temperatures, H_a dominates the resonance behavior, while thermal dephasing "erases" the influence of the anisotropy field in the small size/high temperature limit. An increase in particle size or a decrease in temperature is accompanied by a shift in the resonance field, an increasingly asymmetric line shape, and an increased broadening of the FMR.

If the particles are free to rotate in solution, their easy axes will be oriented in a field. In this case the orientation texture $f(n_\theta, n_\phi, H, T)$ is altered from the isotropic case. The net orientation depends on both temperature and applied field. If a distribution can be frozen into the NP/polymer matrix and the sample is rotated in the spectrometer, the resulting FMR should reflect changes due to the rotating distribution with respect to the applied field.

III. Experimental Methods

Cobalt NPs were prepared, as previously described,[10] by the high temperature decomposition or reduction of organometallic precursors. Structural parameters were confirmed by X-ray powder diffraction and the size distribution was determined by TEM. A comparison of sizes found by X-ray and TEM implies that particles were typically covered with a 0.5 nm oxide layer corresponding to approximately two lattice planes. Magnetic properties were monitored by SQUID magnetometry. The detailed structural study and SQUID magnetometry measurements of cobalt nanoparticles are described elsewhere.[7]

FMR measurements are carried out using an X-band Bruker EPR operating at 9.44 GHz. A modulation field of 10 G and a frequency of 100 kHz were applied. The first derivative of the power adsorption (W) was detected as a function of applied field, and the field range was 0−7000 G. Temperature was controlled using an Oxford Instruments cryostat in the temperature range of 4−300 K, and temperature scans were zero field cooled. The resonance field (H_r) is defined as the field where the derivative of the power is zero ($dW/dH = 0$) and the peak-to-peak distance is the maxima and minima in the derivative signal.

Isolated isotropic distributions of cobalt nanoparticles were prepared by dispersing them in a hexane/paraffin wax solution (Gulf Lite and Wizard Inc). The wax does not exhibit an EPR signal. The hexane was slowly evaporated leaving a solid wax dispersion of particles (~0.2 wt %). Concentration-dependent SQUID and EPR measurements indicate that particles are effectively independent in this dilution regime. However, at substantially higher (but still relatively low) particle concentrations (4 wt % or above), dipolar interactions do become important. For SQUID measurements, we see a decrease in the remnant magnetization at 4% and higher concentrations. Furthermore, those same SQUID measurements of both ϵ-phase and mt-fcc particles reveal nearly identical spectra, indicating that dipolar interactions dominate at high concentrations, wiping out any magnetocrystalline information in the line shape. For the measurements reported here, 0.2% particle/wax composite was transferred to a 4-mm thin wall quartz EPR tube, and the tubes were purged with helium and sealed. In some samples, a comparison of spectra taken before and after the temperature-dependent experiments showed evidence of orientation upon reheating, and those data were discarded. This effect was more pronounced in glass-forming solvents such as methyl cyclohexane and squalene than in waxes. In any case, the spectra presented here showed negligible reorientation upon reheating.

Anisotropic orientation textures were prepared by warming the wax to 40 °C in the presence of a 7000 G field. In this case

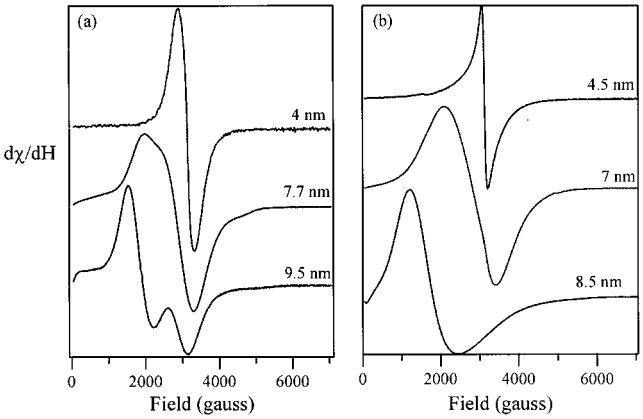

Figure 3. Room-temperature size dependence of FMR spectra of isotropic distributions of cobalt particles isolated in a wax matrix at a 0.2 wt % loading. (a) ϵ-Co, (b) mt-fcc particles.

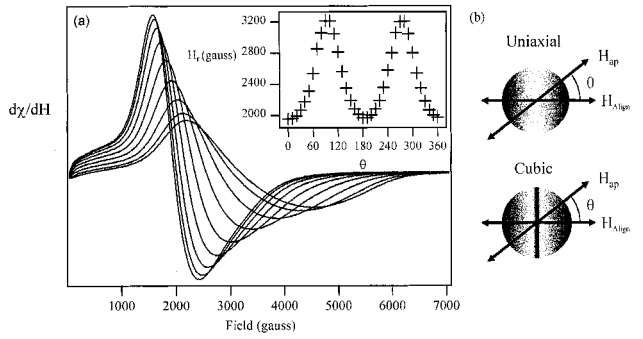

Figure 4. (a) Orientation dependence of the FMR of a dispersion of ϵ-Co particles with an aniostropic orientation texture. The inset (a) is the resonance field as a function of the orientation of the field aligned axis. (b) Schematic representations of the orientation texture for uniaxial and cubic particle dispersions. Shaded regions signify preferred directions of orientation probability, with the highest orientation probabilities shaded the darkest. The projection of the orientation texture on the spectrometer field axis is symmetrical about ϕ when the field-aligned axis is oriented at 0°, and has mirror symmetry when oriented at 90°. The respective symmetries are broken between the two extremes.

the sample is rotated within the cavity and spectra are recorded as a function of angle from the field axis.

IV. Results and Discussion

The measured FMR for both crystal phases follow the general trends predicted by theory. This is evidenced by changing line shapes as the parameter ξ is experimentally adjusted via tuning size (Figure 3), or temperature (Figure 5). Furthermore, manipulation of the superstructure of the particles in the polymer matrix by freezing particles in a field manifests itself in the FMR orientational dependence (Figure 4). Within a mathematical context, this experiment altered the term $f(n_\theta,n_\phi,H,T)$ in eq 4. The comparison of these experiments allowed partial isolation of the dominant physical contribution to FMR. The nearly ideal structure of the ϵ-Co was used as a tool to explore shape and crystal effects that were previously unresolved, while the differing nature of imperfections in the mt-fcc particles allowed us to rationalize our results, especially in light of the body of previous FMR studies on substantially lower quality NPs.

A. Room-Temperature FMR. At room temperature, the magnetization of all of our NPs exhibits rapid thermal equilibration on the time scale of seconds. DC SQUID magnetometry does not detect a remnant magnetization upon removal of an applied field, demonstrating that these particles are superparamagnetic—i.e., the observed magnetization depends on the time

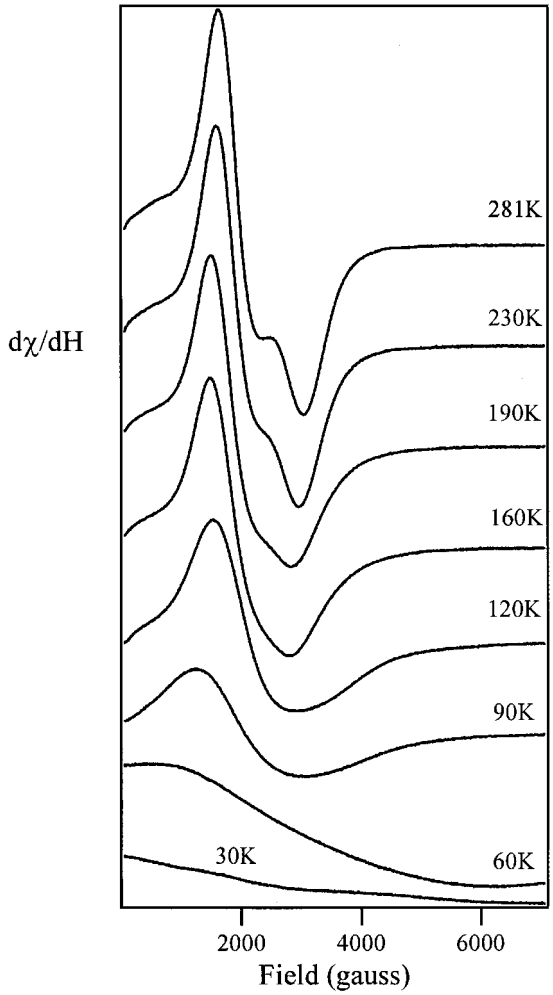

Figure 5. Temperature dependence of the FMR of a dilute, isotropic distribution of 9.5 nm ϵ-Co particles in a wax matrix.

scale over which the system is studied. However, at room temperature, and for the case of large NP's, the FMR spectra do reflect the magnetocrystalline anisotropy within the NP's. In Figure 3 we present FMR results for the case of ϵ-Co and mt-fcc particles. Some expected trends, such as an increase in line shape asymmetry and a shift in the resonance field, are observed as particle size is increased. For the largest NP's of either type, the magnetocrystalline character is reflected in a structured FMR. Thermal dephasing dominates the FMR of the smallest particles, and the resonance is characterized by a single sharp peak at $H_{ap} = \omega/\gamma$. For all samples presented here, rescanning after rotating the sample with respect to the applied field yields identical FMR spectra. This implies that any trends in line shape, recorded as a function of particle size, can be attributable to the structural components that define the net magnetic anisotropy, and are not a result of orientation of the particles. The resolution of features in the FMR of ϵ-Co and the lack of features in the mt-fcc follows from the higher quality crystal structure of the ϵ-Co particles.

For the case of the ϵ-Co, we see the most highly resolved FMR spectra. This resolution arises from both the uniformity of the particle volume and coherence of the crystal lattice. Despite this, there are still significant deviations from spectra generated using the theory of Raikher et al.[8] For example, the spectra of 7.7 nm ϵ-Co contains two features on the low field side of the resonance ($H_{ap} = \omega/\gamma$), and one to the high field side. This is expected for particles with negative cubic anisotropy. We attempted to fit the spectra using a single negative

cubic K_4 as well as a distribution of cubic K_4 values, and we did reproduce the observed spectral features. However, in none of the cases were we able to reproduce their relative intensities. This difficulty is obvious for the 9.5 nm ϵ-Co particles where the high field feature is nearly absent. Efforts to simulate the spectra assuming uniaxial line shapes led to similar difficulties. Furthermore, simulated spectra in which positive anisotropy was assumed required large unphysical shifts in γ to reproduce the line shape.

Discrepancies of the FMR for ϵ-Co from ideal theoretical models are likely due to subtle deviations in particle structure. We know from HRTEM that the ϵ-Co is faceted, leading to non-spherical shapes. Further, micromagnetics calculations indicate that ellipsoidal eccentricities of only a few percent result in anisotropies of the same magnitude as bulk cobalt.[7] In this case, uniaxial shape anisotropy adds otherwise forbidden terms ($l = 2$, K_2) to the FMR line shape function that already contains contributions from the cubic lattice ($l = 4$, K_4). The effective anisotropy is most likely a combination of the observed elliptical (uniaxial) shape as well as cubic magnetocrystalline anisotropy of the lattice. The unique faceting and elongation of each particle serves as a source of broadening of the FMR. On the other hand, the resolution of distinct spectral features suggests there may be a correlation between the crystal lattice and the particle shape. For example, particles may tend to facet along a particular crystal plane to optimize the energy of their surface structure. In this case, shape anisotropy and crystalline anisotropy are isotropic with respect to the spectrometer field, but they are not isotropic with respect to one another. Thus, any relationship between the shape and crystal axes that results from faceting must be explicitly expressed when modeling of the line shape function. However, the unit cell for ϵ-Co is complicated, and it is not obvious from either TEM or X-ray data how best to incorporate such deviations from ideal symmetry. Without a precise basis set for K_{eff}, the zero crossing becomes an unreliable for assignment of a quantitative value for K_{eff}. On the other hand, while the precise magnitude of the components of K_{eff} remain unknown, this result does corroborate the picture of a broad transition temperature and an overall uniaxial anisotropy in a NP with a cubic unit cell, as seen by SQUID magnetometry. Unlike SQUID magnetometry, FMR does provide a distinction between the extents of imperfections of the crystal lattice when comparing the higher crystalline quality ϵ-Co to more structurally complex mt-fcc NP's.

Similar considerations regarding competing shape and crystalline anisotropies also apply to the mt-fcc particles, although, for these particles, crystallographic defects likely play the dominant role in symmetry breaking. As with small ϵ-Co, the 4 nm mt-fcc particles yield a single peak centered at ω/γ. The FMR is inhomogeneously broadened, but this broadening is unlikely to originate from the particle size distribution. Larger particles show a shift in resonance field and significantly broader resonance peaks than what is observed for the smaller mt-fcc particles. This suggests that anisotropy energy is indeed present. In contrast to the ϵ-Co, the FMR in mt-fcc is featureless, similar to what has been previously observed in FMR of magnetic NP's.[11,12] Here, it is likely that the K_a varies from domain to domain within a single particle, so that the effective K_a varies from particle to particle. This effect is highlighted by the fact that a 1% internal strain in a cobalt crystal can change K_a by 60%.[13] For example, a crystal fracture can result in the interconversion of fcc into local regions of the NP possessing a uniaxial hcp lattice with a K_a that is an order of magnitude larger than the cubic phase. As a result, variation between particles within each sample is sufficiently large that any expected fine structure in the FMR is not resolved. Thus, crystallographic imperfections, coupled with shape anisotropy, completely mask the high symmetry of the fcc lattice. Once again, the net result is that the particles yield the characteristic FMR (and DC SQUID) signatures of uniaxial anisotropy.

While both types of particles possess highly uniform volume distributions, the major difference between the ϵ-Co and the mt-fcc particles is that for the ϵ-Co particles, at least some of the unit cell symmetry is manifested in the FMR structure. This difference highlights the fact that while global crystal shape is important in describing the resultant anisotropy of a particle, it is not the whole story. Crystallographic imperfections are equally important for defining the effective easy axes of magnetization in the particles.

B. Orientation. Angular dependent shifts in the resonance field for an anisotropic orientation texture are demonstrated with 9.5 nm ϵ-Co in Figure 4a. Here the resonance field varies sinusoidally (inset), and considerable line broadening occurs when the field-aligned axis is orthogonal to the spectrometer field. The sinusoidal behavior is consistent with net positive uniaxial anisotropy, as predicted in eq 2, while asymmetry may indicate the presence of cubic anisotropy. Line broadening also corroborates the presence of higher order components of K.

To describe the line broadening in Figure 4a, the symmetry of the orientation texture of the dispersion, $f(n_\theta,n_\phi,H,T)$, must be taken into account. Schematic representations are shown for both uniaxial and cubic anisotropies in Figure 4b. In both cases, there is symmetry about the field-aligned axis. However, to account for the line broadening the orientation distribution must be projected onto the field axis of the spectrometer. Rotational symmetry is then lost angles other than $\theta = 0°$, while mirror symmetry is regained at $\theta = 90°$. Taking into account this symmetry, as well as the fact that H_r changes slowly about θ in parallel and orthogonal configurations, uniaxial particles should have the narrowest line widths at 0° and 90°, and broad line widths in between. This is not the case for the ϵ-Co particles, where the line broadening is greatest at 90°. This is most likely due to cubic components of the anisotropy for the ϵ-Co particles. For cubic anisotropy, the orientation texture is sampling all values for ϕ in eq 3 at field-aligned configurations orthogonal to the spectrometer axis. As seen in Figure 4, this would make the line broadening largest at $\theta = 90°$.

The existence of multiple anisotropy components is evident from the orientation-dependent FMR. However, the dominance of positive anisotropy inherent to the particle itself is by no means certain. The fitting of FMR spectra of oriented cubic domains is often riddled with mathematical difficulties.[14] These complications are exacerbated by the knowledge of competing anisotropies. Here, the particle will orient in a field to its effective anisotropy axis due to both shape and crystalline contributions, making it difficult to determine the orientation texture with respect to the individual anisotropy components. Second, the net orientation texture is likely to be anisotropic with respect to the distribution of anisotropies in the particle matrix—i.e., particles with a larger anisotropy field due to more exaggerated deviations from a spherical shape should align more easily with the applied field. Finally, it is possible that the particles suspended in a liquid matrix will aggregate in the presence of an applied field. We base this presumption on the fact that we have used moderate magnetic fields to both orient and align particles as well as separate particles of differing size. Dipole interactions between particles are long range, and are

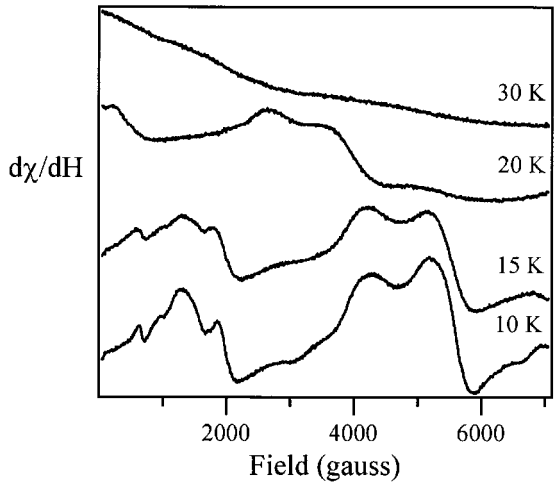

Figure 6. Low-temperature FMR of ϵ-Co. The complex, temperature-dependent structure is interpreted as evidence for surface magnetic effects.

observed to influence both FMR and SQUID magnetometry in relatively dilute regimes.[7,15]

Again, our ability to control crystallographic morphology and particle size gives us particles that are far superior when compared with those that have been previously utilized in similar FMR studies. This gives us insight into the highly complex nature of magnetocrystalline anisotropy in finite-sized ferromagnets, which is not readily understood within the context of existing models. The competition between particle shape and crystalline anisotropy, which is partially resolved here, is not measurable in poorer quality samples.

C. Temperature Dependence. Resolution of anisotropy, and hence spectral features, is also significant in FMR at low temperatures. Here, decreasing temperature should generate trends that are analogous to what are observed for increasing NP size. Temperature-dependent FMR measurements are typically used to determine K_a by looking at the change in H_r as a function of temperature. Such measurements are often combined with orientation dependence in which the particles are field-cooled to generate a net-alignment, and then the FMR is recorded at various sample orientations.[16,17] In contrast to theory, the temperature dependence of ϵ-Co is marked by a disappearance of structural information with decreasing temperature and, eventually, a significant broadening is observed (Figure 5). These trends are explained by the fact that, at lower temperatures, the particle moments are unable to overcome the local anisotropy barriers and, thus, become trapped in metastable states. At temperatures where k_bT is much greater than the anisotropy barriers, thermal fluctuations ensure that the particles relax back to their equilibrium configuration after they are perturbed by the microwave field. *This is the regime where the model of Raikher et al. is applicable.* The use of dc SQUID magnetometry indicates that nonequilibrium behavior persists over long time scales ($t \sim 120$ s) when the particles are at moderately low temperatures and fields, as seen in Figure 4. More accurate measurements of low-temperature FMR in these NP's would require higher frequency/field spectrometers than are commonly available.

D. Surface Effects. The FMR of ϵ-Co at low temperatures exhibits a transformation first to extremely broad resonances with an accompanying shift in the 0-crossing field, and then, below 35 K, much narrower features appear and shift to higher field (Figure 6). The resolution of narrow features below 35 K is reproducible in the ϵ-Co, but does not appear in the mt-fcc particles. As discussed below, these sharp features are most likely due to surface effects. Surface effects in FMR have been the more recent theoretical focus of Raikher et al.[16] as well as Aharoni.[17,18] To our knowledge, a FMR spectrum has not been previously reported for surface effects in nanoparticles.

The surface of the ϵ-Co particles is a diverse structural and chemical environment that includes uncompensated spins, vacancies, and an oxide interface. As previously mentioned, X-ray data indicates the dominance of a cobalt monoxide layer. However, the surface is most likely characterized by a mixed oxide. The cobalt monoxide phase is expected to be antiferromagnetic with a low Néel temperature, $T_N = 33$ K. As a comparison, we have conducted room temperature experiments on chromium nanoparticles. Here the metallic phase is antiferromagnetic and the oxide phase is ferromagnetic. With controlled oxidation of the particles, we see an analogous change in the FMR to the low temperature dependence. In metallic Cr particles, the FMR behavior nearly matches that of the low temperature ϵ-Co data, while the oxide phase behaves as a standard ferromagnet. As for the cobalt, the appearance of the low-temperature FMR features does seem to coincide with the bulk Néel temperature, although it is not clear whether the Néel temperature should be sensitive to finite size effects.

Neglecting the oxide, the surface anisotropy should be strongly correlated to the crystallographic nature of the particle. At the interface, changes in the nature of the bulk spin−orbit coupling are disrupted and the symmetry of the bulk at the surface is reduced. Raikher et al. have reported shifts in the resonance fields, which they attribute to canted spins at the surface of magnetite particles.[16] The nature of the anisotropy at the surface should depend on the symmetry of the underlying bulk crystal lattice. Consequently, the crystal structure of the particle and the extent of imperfections should affect the net surface anisotropy. For example, similar surface effects may be present for the mt-fcc particles, but remain masked by sample inhomogeneity.

V. Conclusions

The magnetic properties of a NP ensemble are acutely sensitive to structural components of the particle. This is seen in particle dispersions where inhomogeneity due to volume distributions can be nearly neglected. Here, both shape and crystallographic anisotropy contribute to the effective anisotropy of a NP. By comparing the FMR from crystalline magnetic NP's to magnetic NP's with imperfect structure it is apparent that the coherence of the lattice is equally important in describing the anisotropy and hence inhomogeneity of the magnetic properties of the NP's. The ability to separate these factors sheds light on the interpretation of orientation and temperature dependent FMR techniques. Finally, surface effects are revealed at lower temperatures. In summary, FMR is a sensitive probe of crystallographic imperfection, particle shape, and surface composition. With magnetic recording media approaching nanometer length scales, and as data transfer rates continue to increase, explicit control over NP structure and over the high frequency response of NP's will become increasingly important.

Acknowledgment. This work was supported through an NSF GOALI grant.

References and Notes

(1) Bean, C. P.; Livingston, J. D. *J. Appl. Phys.* **1959**, *30*, 120S.
(2) Neel, L. *Ann. Geophys.* **1949,** *5*, 99.

(3) Brown, W. F. *Phys. Rev.* **1963,** *130*, 1677.
(4) Dinega, D. P.; Bawendi, M. G. *Angew. Chem.* **1999**, *38* (12), 1788.
(5) Hall, B. D.; Monot R. Comput. Phys. **1991**, *5*, 414−417.
(6) Hall, B. D.; Flueli, M.; Monot, R.; Corel, J.-P. *Phys. Rev. B* **1991**, *43*, 3906−3917.
(7) Held, G. A., et al. Submitted.
(8) Raikher, Y. L.; Stepanov, V. I. *Sov. Phys. JETP* **1992**, *75*, 764−771.
(9) Raikher, Y. L.; Stepanov, V. I. *Phys. Rev. B* **1994**, *50*, 6250−6259.
(10) Sun, S., et al. In press.
(11) Saenger, J. F.; Neto, K. Skeff; Morais, P. C.; Sousa, M. H.; Tourinho, F. A. *J. Magn. Reson.* **1998,** *134*, 180−183.
(12) Gazeau, F.; Shilov, V.; Bacri, J. C.; Dupois, E.; Gendron, F.; Perzynski, R.; Raikher, Yu. L.; Stepanov, V. I. *J. Magn. Magn. Mater.* **1999**, *202*, 535−546.
(13) Back, C. H.; Weller, D.; Heidmann J.; Mauri, D.; Guarisco, D.; Garwin, E. L.; Siegmann, H. C. *Phys. Rev. Lett.* **1998**, *81*, 3251−3254.
(14) Vonsovskii, S. V. *Ferromagnetic Resonance*; Pergamon Press: New York, 1966.
(15) Hrianca, I.; Malaescu, F.; Claici, F.; Marin C. N. *J. Magn. Magn. Mater*. **1999**, *201*, 126−128.
(16) Shilov, V. I.; Raikher, Y. L.; Bacri, J.-C.; Gazeau, F.; Perzynski, R. *Phys. Rev. B* **1999**, *60*, 11902−11905.
(17) Aharoni, A. *J. Appl. Phys.* **1987**, *61*, 3302.
(18) Aharoni, A. *J. Appl. Phys*. **1997**, *81*, 830.